CHAPTER 2

WAVE-CURRENT INTERACTION IN HARBOURS

Jan K. Kostense, Maarten W. Dingemans and Peter Van den Bosch[*]

ABSTRACT

A finite element model has been developed to study the effect of currents on the wave propagation in and around arbitrarily shaped harbours of variable depth. The model solves an elliptic mild-slope type of equation for time-harmonic waves, and thus circumvents the limitations of existing models for wave-current interaction in coastal areas, which apply a parabolic approximation. Numerical examples are presented, both for schematized cases, as the effect of "rip currents" on normal incident waves on a sloping beach, and for a realistic geometry.

1. INTRODUCTION

An effective tool to study the wave penetration into harbours of variable depth and arbitrary shape is the mild-slope equation as originally derived by Berkhoff (1972). The equation describes the combined effect of bottom refraction and diffraction on the propagation of linear gravity waves. Booij (1981) suggested how to extend the equation to account for dissipative effects. To solve the full elliptic equation, Kostense et al. (1986) presented a finite-element model, which has been implemented with several types of boundary conditions, such as partial reflection, and combined reflection and transmission. They experimentally verified their model for a complex harbour geometry, and showed that it can be successfully applied, for instance to study the dissipative effects of bottom friction and permeable breakwaters on harbour resonances. The implementation of wave breaking in the model is described by De Girolamo, Kostense and Dingemans (1988), while the numerical solution methods are discussed by Hurdle, Kostense and Van den Bosch (1989). The

[*] Delft Hydraulics, P.O. Box 152, 8300 AD Emmeloord, the Netherlands

model has been implemented on two different supercomputers, viz. a Cray XMP and a NEC SX/2. Taking advantage of its vector-processors, the system of equations is solved quite efficiently, enabling computations of relatively large areas.

Radder (1979) introduced a parabolic approximation of the mild-slope equation and thus converted a boundary value problem into an initial value problem. The nature of the parabolic approximation is such that diffraction and reflection are neglected in the computational main-wave propagation direction. Since then, this technique was widely applied to study the wave propagation in coastal areas, especially after Booij (1981) introduced an extended equation accounting for the effect of varying currents. Kirby (1984) showed that Booij used an improper form of the dynamic free surface boundary condition, and derived an improved equation.

Apart from coastal regions, currents may also have a noticeable effect on the wave penetration into harbours, especially if they are situated in tidal inlets, in estuaries, near in- and outlets of power plants, etc. Until now this effect could not be incorporated in numerical studies, as parabolic methods inhibit reflections opposite to the main direction of wave propagation. Therefore, the finite element model pre-sented by Kostense et al. (1986) has been modified to solve the equation as derived by Kirby (1984). The model has been given in section 2 and the necessary iteration procedure for the wave direction has been described in section 3. To illustrate the effectiveness of the model, in section 4 a series of computations is discussed, both for schematized cases, and for a realistic geometry.

2.   THE EXTENDED MILD-SLOPE EQUATION

For irrotional wave motion, the velocity potential $\Phi(\vec{x}, z, t)$ is written as

$$\Phi(\vec{x}, z, t) = f(z, h) \ \phi(\vec{x}, t) \quad \text{with} \tag{1}$$

$$f(z, h) = \frac{\cosh[k(h+z)]}{\cosh kh} \ . \tag{2}$$

With an ambient current field $\vec{U}(\vec{x})$ the time-dependent mild-slope

equation results as (Kirby, 1984)

$$\frac{D^2\phi}{Dt^2} + \left(\nabla\cdot\vec{U}\right)\frac{D\phi}{Dt} + \phi\frac{D}{Dt}(\nabla\cdot\vec{U}) - \nabla\cdot(cc_g\nabla\phi) + (\omega_r^2 - k^2cc_g)\phi = 0 \ , \tag{3}$$

where c, c_g and k represent the phase velocity ω_r/k , the group velocity $d\omega_r/dk$, and the wave number $|\vec{k}|$, respectively, ∇ is the two-dimensional gradient operator, and further

$$\frac{D}{Dt} \equiv \frac{\partial}{\partial t} + \vec{U}\cdot\nabla \ , \qquad . \tag{4}$$

$$\omega_r = \omega - \vec{k}\cdot\vec{U} \ , \quad \text{and} \quad \omega_r^2 = gk \tanh kh \ . \tag{5a,b}$$

Introducing time-harmonic motion,

$$\phi(\vec{x}, t) = Re\left\{\psi(\vec{x})e^{-i\omega t}\right\} \ , \tag{6}$$

there results

$$\frac{\partial}{\partial x_i}\left[cc_g\frac{\partial\psi}{\partial x_i} - U_iU_j\frac{\partial\psi}{\partial x_j}\right] + 2i\omega U_j\frac{\partial\psi}{\partial x_j} + \left(k^2cc_g + \omega^2 - \omega_r^2 + i\omega\nabla\cdot\vec{U}\right)\psi = 0 \ . \tag{7}$$

The equation solved in the finite element model is obtained from Eq. (7) by assuming currents which are small compared to the group velocity, and thus neglecting the quadratic term in U. Furthermore, at the right-hand side of the equation the dissipation term is added (see also Hurdle et al., 1989):

$$\frac{\partial}{\partial x_j}\left[cc_g\frac{\partial\psi}{\partial x_j}\right] + 2i\omega U_j\frac{\partial\psi}{\partial x_j} + \left(k^2cc_g + \omega^2 - \omega_r^2 + i\omega\nabla\cdot\vec{U}\right)\psi = -i\omega_r W\psi \ . \tag{8}$$

The equation is solved by means of standard finite element techniques, using triangular elements with linear interpolation functions.

3.   ITERATION PROCEDURE FOR CURRENT EFFECT

As the relative wave frequency, ω_r, is dependent on the unknown direction of $\vec{k}$, Eq. (8) can be solved only in an iterative manner. To elucidate the iteration procedure and its underlying assumptions, the case of a traveling wave is considered:

$$\psi(\vec{x}) = b(\vec{x}) \; e^{iS(\vec{x})} \; . \tag{9}$$

Inserting this expression into Eq. (8) results into an energy transport equation and the eikonal equation:

$$(\nabla S)^2 = k^2 + \frac{\nabla c c_g}{c c_g} \cdot \frac{\nabla b}{b} + \frac{\nabla^2 b}{b} + \frac{1}{c c_g}\left[(\omega - \vec{U} \cdot \nabla S)^2 - \omega_r^2\right] \; . \tag{10}$$

Since the phase function of ϕ reads $\chi(\vec{x}, t) = S(\vec{x}) - \omega t$, the wave number vector as resulting from the (extended) mild-slope equation can be obtained as

$$\vec{\kappa} = \nabla\chi = \nabla S \; . \tag{11}$$

It is stressed that the absolute value, k, of the initial wave number results as a constant due to the separation of variables in Eq. (1), which splits off the vertical structure from the wave propagation space. Equation (10) shows that in the wave propagation space the absolute value of the wave number vector κ is different from k due to the effects of bottom slope (through $\nabla c c_g / c c_g$), of diffraction (through $(\nabla^2 b)/b$), and of currents. The unknown direction of $\vec{\kappa}$ in the Doppler-shift equation (5a) is now approximated by the resulting direction of $\vec{\kappa}$, resulting from the former iteration step.

The iteration procedure runs as follows. For the first step the relative wave frequency ω_r in Eq. (5a) is obtained assuming either $\vec{U} = 0$, or a direction of $\vec{\kappa}$ equal to the incident wave direction. Then Eq. (8) yields the solution ψ_0 and the wave number vector

$$\vec{\kappa}_0 = \nabla S = Im\left(\frac{\nabla\psi_0}{\psi_0}\right) \; . \tag{12}$$

For the second step the direction of $\vec{\kappa}_0$ is used as an estimate for the direction of $\vec{\kappa}$ in Eq. (5a)

$$\omega_r = \omega - \left(\frac{\vec{\kappa}_0}{\kappa_0} k\right) \cdot \vec{U} \; , \tag{13}$$

from which, together with the dispersion relation (5b), ω_r and k can be solved and substituted into the mild-slope equation. Now the solution

ψ_1, which yields from the second step, is used to determine $\vec{\kappa}_1$ and ω_r from expressions similar to Eqs. 12 and 13. From hereon the iteration process continues till a certain accuracy is achieved. To determine whether the stopping criterion is met, the procedure is essentially the same as applied for problems involving dissipation, where the magnitude of W is dependent on the local wave potential, see also Kostense et al. (1986) and De Girolamo et al. (1988). The number of occurrences for which the successive iterations of ψ_n differ more than some relative amount from ψ_{n-1} are counted. This is carried out separately for the real and the imaginary part for each of the mesh points:

if $\quad \left| \dfrac{Re(\psi_n) - Re(\psi_{n-1})}{Re(\psi_n)} \right| > \varepsilon \quad$ then $\quad N_e = N_e + 1$

and also

if $\quad \left| \dfrac{Im(\psi_n) - Im(\psi_{n-1})}{Im(\psi_n)} \right| > \varepsilon \quad$ then $\quad N_e = N_e + 1$

Here ε is a predetermined accuracy of a few percents. With N_e occurrences at a total of N mesh points, the iteration is stopped when $N_e/N < 0.01$. Because the real and the imaginary parts are counted separately, deviations may occur in less than 0.5 % of the mesh points. To obtain reliable estimates of $\nabla\psi$ in Eq. 12, a minimum number of about 12 mesh elements per wave length is required. This condition is essentially the same as for bottom friction computations, which also involve the assessment of $\nabla\psi$, see Kostense et al (1986). Fulfilling this condition, usually about 5 iterations appear to be adequate to obtain reliable results of wave-current computations.

4.0 NUMERICAL EXAMPLES

As numerical examples have been selected wave propagation over a rip current, over a vortex ring and, as an example of a realistic geometry, wave penetration in the Malamocco inlet to the Venice Lagoon.

Rip current

To demonstrate the application of the model to wave-current interactions, computations were performed on the effect of a rip current

on the propagation of normally incident waves on a plane beach with a slope of 1/50, a problem that was originally studied by Arthur (1950). The velocity field is given by

$$U_x = -3.60 \left[2 - \left(\frac{y}{76.2} \right)^2 \right] F\left(\frac{y}{76.2} \right) \int_0^{\frac{x}{7.62}} F(\sigma) d\sigma$$

$$U_y = 0.4731 \ y \ F\left(\frac{y}{76.2} \right) F\left(\frac{x}{7.62} \right)$$

with

$$F(\sigma) = (1/\sqrt{2\pi}) \ \exp(-\sigma^2/2)$$

and is illustrated in Fig. 1. This Figure also shows Arthur's results for a wave period of 8 seconds. These results were obtained with the ray approximation method, which allows for refraction and shoaling only and thus yields unlimited wave heights where the rays cross each other.

Fig. 2 shows two wave height distributions – without and with the effect of wave breaking – obtained from the finite element model. For these computations a grid of 74,003 nodes was used. For nonbreaking and breaking conditions, the computations required 5 and 8 iterations, respectively. The conditions are the same as applied by Arthur. To quantify the effect of wave breaking the formulation given by Battjes and Janssen (1978) has been used, see De Girolamo et al. (1988). Comparing both wave height distributions, the inclusion of wave breaking appears to yield more stable results.

It should be noted that the results in Fig.2 could have been approximated satisfactory by parabolic models, see e.g. Kirby (1983). The reason to perform these computations was to show that nowadays super-computers enables one to cope with relatively large areas, to which one would have been compelled by the presence of any reflective constructions, such as groynes.

Vortex ring

The model has also been applied to study the wave propagation over a vortex ring in constant water depth. Examples of the occurrence of
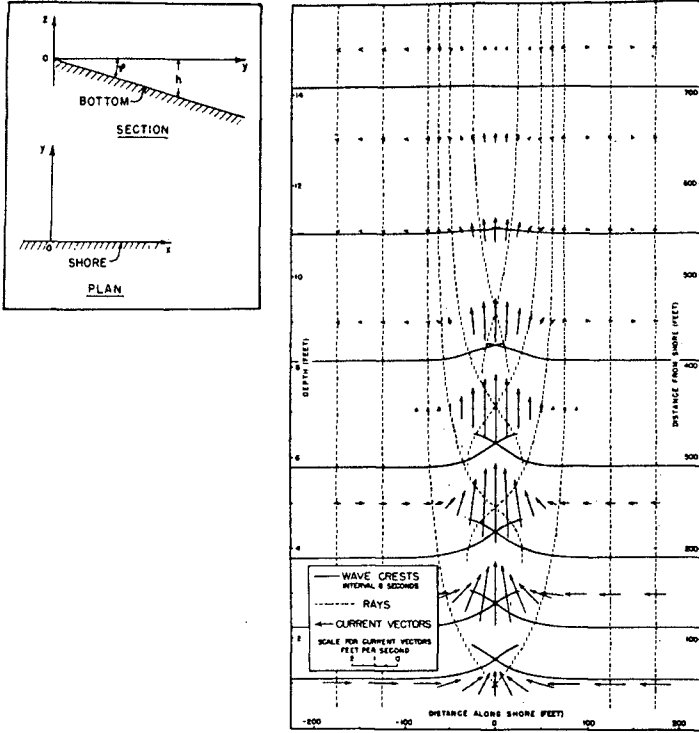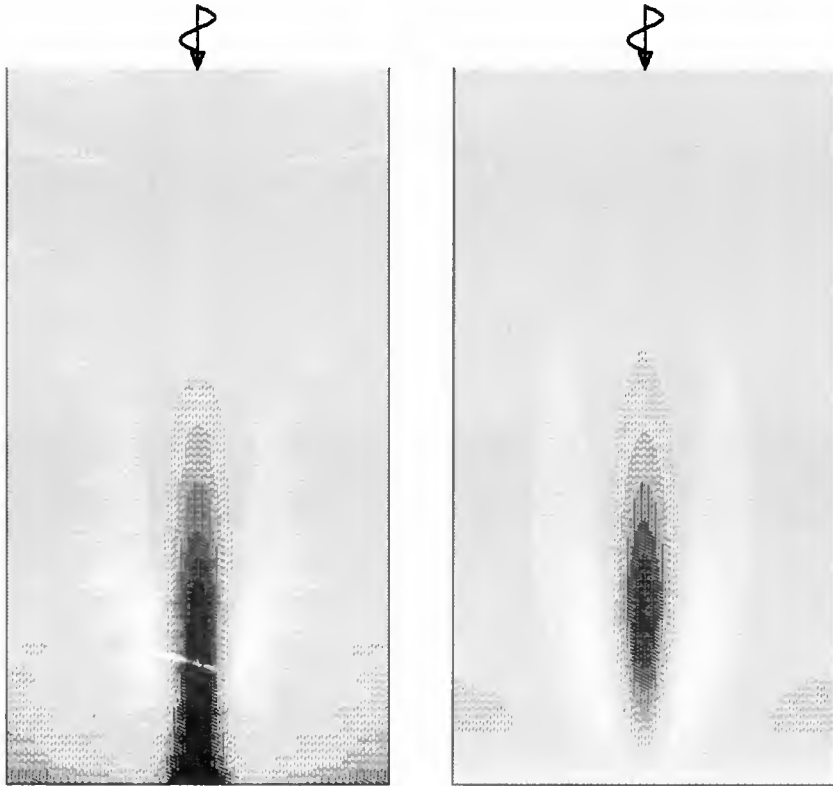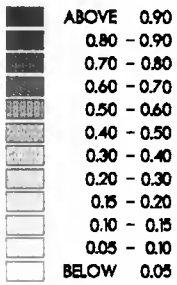
Figure 1 Typical rip current, from Arthur (1950)

without breaking   with breaking

ABOVE 0.90
0.80 – 0.90
0.70 – 0.80
0.60 – 0.70
0.50 – 0.60
0.40 – 0.50
0.30 – 0.40
0.20 – 0.30
0.15 – 0.20
0.10 – 0.15
0.05 – 0.10
BELOW 0.05

Wave height in m

Hs = 0.20 m
T = 8.0 s

Figure 2   Rip current; wave height distributions without and with
           breaking

vortex rings in nature are the Gulf stream warm-core rings and the large-scale vortices along the Norwegian coast. The finite element grid, which was used for this study consisted of 114,661 nodes, representing a circular area with a diameter of 5 km. The shape of the current velocity distribution is essentially the same as applied by Yoon (1987): the radial velocity component $V_r = 0$ and the tangential velocity given by

$$V_\theta = C_1 \left(\frac{r}{R_1}\right)^N \qquad\qquad \text{for } r \leq R_1 \text{ , and}$$

$$V_\theta = C_2 \exp\left[-\left(\frac{R_2 - r}{R_3}\right)^2\right] \qquad\qquad \text{for } r > R_1.$$

The maximum velocity C_2 occurs along the circle $r = R_2$. For the numerical computation the coefficients were taken to be $C_1 = 0.9$ m/s, $C_2 = 1.0$ m/s, $R_1 = 900$ m, $R_2 = 1000$ m, $R_3 = 300$ m and $N = 2$. Fig. 3 shows the current velocity distribution, which rotates clockwise. For a water depth of 100 m, a wave period of 10 seconds and an incident wave height of 1.0 m the wave height distribution resulting from a computation without dissipation is shown in Fig. 4. The computation required 7 iterations. In the lower part of the graph the wave directions diverge due to current refraction, resulting in low waves. This area is bounded by a caustic line, where the refracted waves interact with the undisturbed ones. Diffraction in lateral direction precludes unlimited wave heights along this line. The consecutive caustic lines in the upper part of the graph originate from converging wave directions.

Malamocco inlet to the Venice Lagoon

An example from engineering practice of the effect of an ambient current is the wave penetration of the Malamocco inlet to the Venice Lagoon, which was computed as part of the project to develop a flood defence system for Venice. The schematization of the inlet and the bottom topography, as well as a representative ebb current field, are illustrated in Fig. 5. The computational grid comprised 249.088 nodes. The wave field was computed for a water level of CD + 0.80 m, representing mean sea level, and for waves incident from a bearing of 137°N with a height of 1.8 m and a period of 8 seconds.
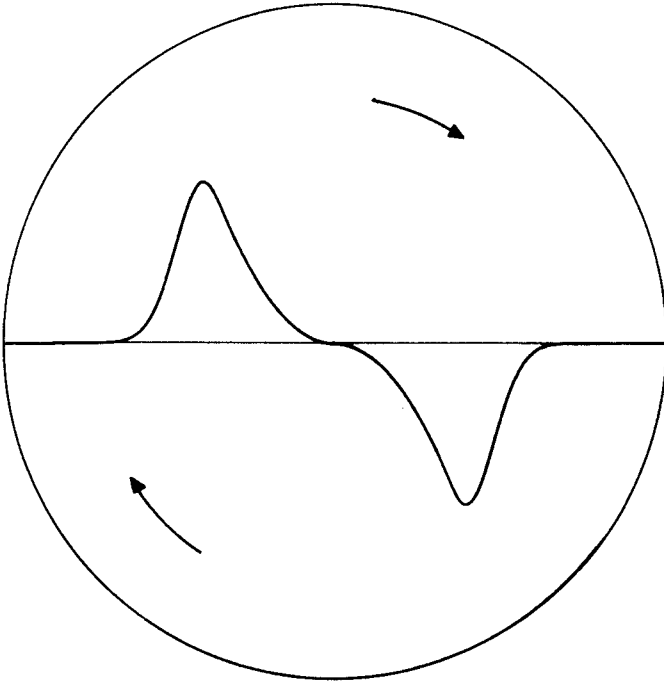
$$V_r = 0$$

$$V_\theta = C_5 \left[\frac{r}{R_1} \right]^N \qquad \text{for } r < R_1$$

$$V_\theta = C_6 \exp \left[-\left(\frac{R_2 - r}{R_3}\right)^2 \right] \qquad \text{for } r \geqslant R_1$$

with:

$C_5 = 0.9$ m/s
$C_6 = 1.0$ m/s
$R_1 = 900$ m
$R_2 = 1000$ m
$R_3 = 300$ m
$N = 2$

Figure 3   Vortex ring; current velocity profile
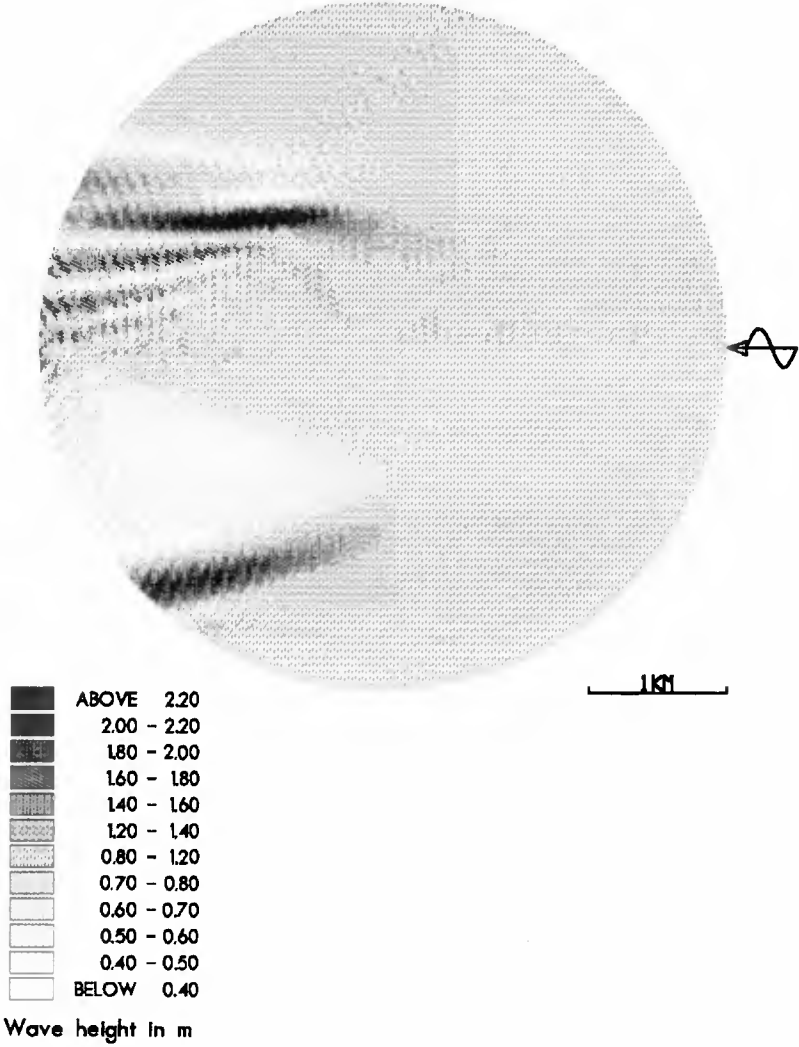
Figure 4   Vortex ring; wave height distibution

bottom topography

ABOVE   30.00
20.00 – 30.00
15.00 – 20.00
13.00 – 15.00
11.00 – 13.00
9.00 – 11.00
7.00 – 9.00
5.00 – 7.00
3.00 – 5.00
1.00 – 3.00
BELOW   1.00

Water depth in m

1KM   ↑ N

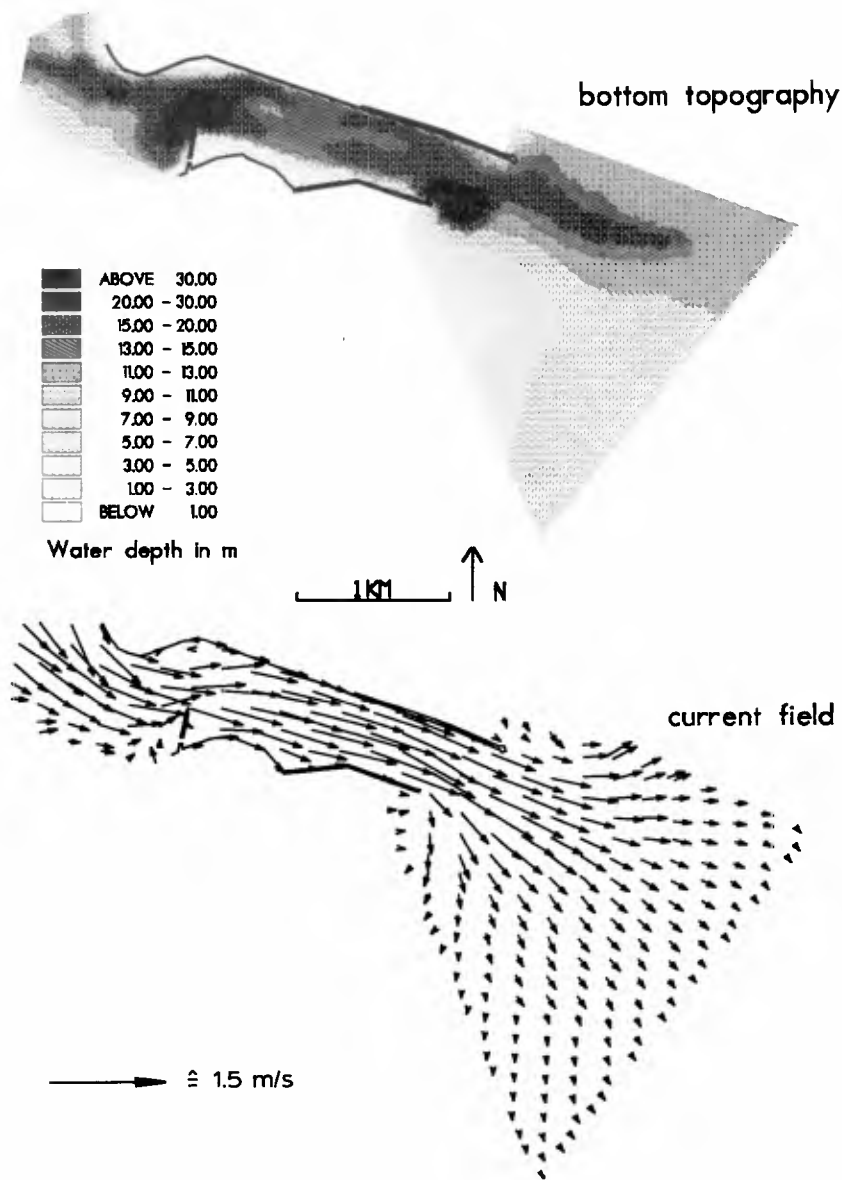current field

⇒ 1.5 m/s

Figure 5   Malamocco inlet to the Venice lagoon area;
bathymetry and typical ebb currents

The results, with and without current, are shown in Figure 6. The wave height distribution for the no current case shows a focussing of energy along the south side of the entrance channel due to so-called channel refraction. This also results in a reduction of the wave height in the channel region. The inclusion of the ebb current in the computation results in a significant increase in penetration of the inlet. This is due to the the effects of current refraction, which offset the effects of bottom refraction on the south slope of the channel. The computation with current required 4 iterations and was executed on a NEC SX/2. The required CPU time was 42 minutes at a performance of 250 Mflop/s.

5. DISCUSSION

The effect of ambient currents on wave propagation in and around harbours and coastal regions with reflective boundaries can be determined by means of a finite element model solving an extended mild-slope equation. Contrary to the original mild-slope equation for bottom refraction and diffraction only, the extended equation should be solved in an iterative way, as beforehand the wave direction in the computational region is unknown. Apart from the strength of the currents, the number of iterations depends on the number of elements per wave length. For stability reasons a minimum number of about 12 elements per characteristic wave length is required to obtain accurate estimates of the gradient of the velocity potential. This number is essentially the same as applied for the dissipative effects of bottom dissipation, see Kostense et al. (1986). For non-iterative computations without currents and dissipation the number of elements is determined by the desired accuracy; for engineering purposes usually about 8 elements per characteristic wave length are applied.

The presented numerical examples show that the extended model successfully integrates the effects of diffraction, bottom refraction, current refraction, reflection and dissipation. Moreover, it is shown that even relatively weak currents may have a significant influence on the wave propagation.

6. ACKNOWLEDGEMENT

The case study results shown in Fig.6 were established within the scope

Offshore conditions:

Wavehght Hs = 2.0   m

Direction = 140   deg

Period   Tp =   8.0 s

Water level = +0.8 m

no flow

1KM   ↑ N

ABOVE   2.50
2.00 – 2.50
1.50 – 2.00
1.25 – 1.50
1.00 – 1.25
0.75 – 1.00
0.50 – 0.75
0.40 – 0.50
0.30 – 0.40
0.20 – 0.30
0.10 – 0.20
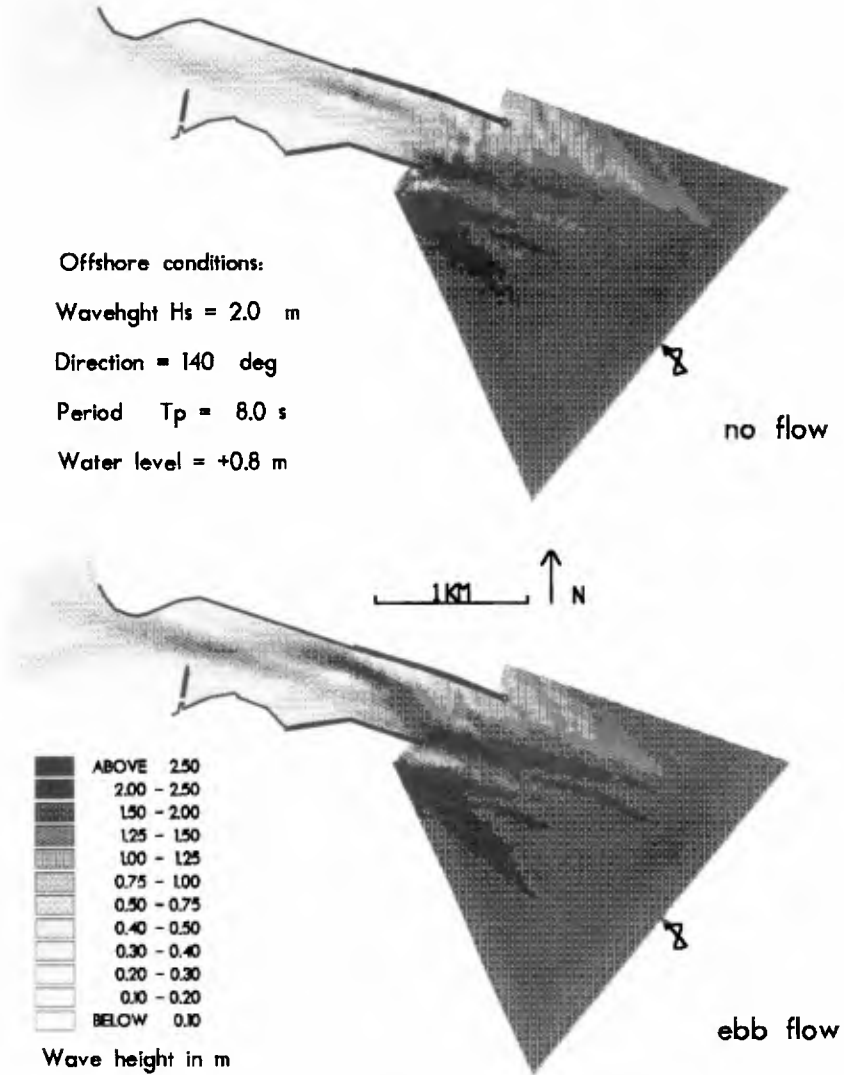BELOW   0.10

Wave height in m

ebb flow

Figure 6   Malamocco inlet to the Venice lagoon area; effect of
an ambient current field on the wave height distribution

of a study of the wave behaviour at the Venice Lagoon inlets, which study was commissioned to Delft Hydraulics by Consorzio VENEZIA NUOVA.

7. REFERENCES

Arthur, R.S., 1950: Refraction of shallow water waves: the combined effect of currents and underwater topography; Trans. Am. Geoph. Union, Vol. 31, No. 4, pp. 549-552.

Battjes, J.A. and Janssen, J.P.F.M., 1978: Energy loss and set-up due to breaking of random waves; Proc. 16th Int. Conf. Coastal Engng., Hamburg, pp. 569-587.

Berkhoff, J.C.W., 1972: Computation of combined refraction-diffraction; Proc. 13th Int. Conf. Coastal Engng., Vancouver, pp. 471-490.

Booij, N., 1981: Gravity waves on water with non-uniform depth and current; Communications on Hydraulics, Dept. of Civil Engng., Delft Univ. of Techn., Rep. no. 81-1.

De Girolamo, P., Kostense, J.K. and Dingemans, M.W., 1988: Inclusion of wave breaking in a mild-slope model; in Proc. Int. Conf. Computer Modelling in Ocean Engng., Venice.

Hurdle, D.P., Kostense, J.K. and Van den Bosch, P., 1989: Mild-slope model for the wave behaviour in and around harbours and coastal structures in areas of variable depth and flow conditions; Proc. 2nd Int. Symp. Water Modelling and Measurement, Harrogate, England.

Kirby, J.T., 1983: Propagation of weakly-nonlinear surface water waves in regions with varying depth and current; Univ. Delaware, Newark, U.S.A., Research rep. no. CE-83-37

Kirby, J.T., 1984: A note on linear surface wave-current interaction over slowly varying topography; J. Geophys. Res., Vol. 89, No. C1, pp. 745-747.

Kostense, J.K., Meijer, K.L., Dingemans, M.W., Mynett, A.E. and Van den Bosch, P., 1986: Wave energy dissipation in arbitrarily shaped harbours of variable depth; Proc. 20th Int. Conf. Coastal Engng., Taipei, pp. 2002-2016.

Radder, A.C., 1979: On the parabolic equation method for water wave propagation; J. Fluid Mech., Vol. 95, No. 1, pp. 159-176.

Yoon, S.B., 1987: Propagation of shallow-water waves over slowly varying depth and currents; thesis Cornell Univ., U.S.A.